

# Opportunity of Spinel Ferrite Materials in Nonvolatile Memory Device Applications Based on Their Resistive Switching Performances

Wei Hu, Ni Qin, Guangheng Wu, Yanting Lin, Shuwei Li, and Dinghua Bao\*

State Key Laboratory of Optoelectronic Materials and Technologies, School of Physics and Engineering, Sun Yat-Sen University, Guangzhou 510275, China

## S Supporting Information

**ABSTRACT:** The opportunity of spinel ferrites in nonvolatile memory device applications has been demonstrated by the resistive switching performance characteristics of a Pt/NiFe<sub>2</sub>O<sub>4</sub>/Pt structure, such as low operating voltage, high device yield, long retention time (up to 10<sup>3</sup> s), and good endurance (up to 2.2 × 10<sup>4</sup> cycles). The dominant conduction mechanisms are Ohmic conduction in the low-resistance state and in the lower-voltage region of the high-resistance state and Schottky emission in the higher-voltage region of the high-resistance state. On the basis of measurements of the temperature dependence of the resistances and magnetic properties in different resistance states, we explain the physical mechanism of resistive switching of Pt/NiFe<sub>2</sub>O<sub>4</sub>/Pt devices using the model of formation and rupture of conducting filaments by considering the thermal effect of oxygen vacancies and changes in the valences of cations due to the redox effect.

Recently, resistive random access memory (RRAM) based on resistive switching effects has attracted considerable attention for the next generation of nonvolatile memory devices because of its nonvolatility, high-density integration, high operation speed, low power consumption, and good compatibility with complementary metal oxide semiconductor processing.<sup>1–5</sup> The resistive switching memory cell is usually built in the capacitor-like metal/insulator/metal (MIM) configuration, where the insulator acts as the active layer for resistive switching. After so-called electroforming, the MIM memory cell can be switched reversibly between at least two different resistance states, including high-resistance state (HRS) and low-resistance state (LRS). There are two types of resistive switching effects. One is unipolar resistive switching, whose switching process depends on the magnitude of the electric field rather than on the polarity of the external voltage, the other is, in contrast, bipolar resistive switching, which requires reversal of the polarity of the external voltage.<sup>1,2</sup>

Although numerous materials such as metal oxides,<sup>4–8</sup> chalcogenide materials,<sup>9</sup> and carbon-based materials<sup>10</sup> have been used as the active layer (“I”) in the MIM structure, several reliability issues, including nonuniform dispersion of the switching parameters, high electroforming voltage, and low device yield, need to be solved.<sup>11</sup> Meanwhile, the physical mechanism of resistive switching is still controversial. Therefore, remarkable efforts have been directed to the search for

new resistive switching materials and understanding the physical origin of resistive switching.

As one of the most versatile and technologically important ferrite materials, spinel ferrite, NiFe<sub>2</sub>O<sub>4</sub>, has been intensively investigated for its rich electronic and magnetic properties. It has been widely used in electromagnetic devices and magnetic components such as resonators, phase shifters, spintronics devices, and gas and humidity sensors.<sup>12–15</sup> In our previous work, thin films of the spinel-like structure MgZnO were found to exhibit excellent resistive switching effects.<sup>16</sup> Therefore, whether thin films of real spinel ferrite materials such as NiFe<sub>2</sub>O<sub>4</sub> could show resistive switching effects becomes an interesting topic. Although NiFe<sub>2</sub>O<sub>4</sub>/SrTiO<sub>3</sub>:Nb junctions were reported to exhibit resistive hysteresis due to charge accumulation at the interfaces stemming from the interfacial capacitance effect,<sup>17</sup> the utilization of NiFe<sub>2</sub>O<sub>4</sub> thin films with unipolar resistive switching performance, which is completely different from the interfacial charge accumulation of the NiFe<sub>2</sub>O<sub>4</sub>/SrTiO<sub>3</sub>:Nb junctions, to fabricate RRAM has not been reported. Herein we report the unipolar resistive switching behavior of Pt/NiFe<sub>2</sub>O<sub>4</sub>/Pt memory devices. On the basis of the temperature dependence of the resistance and the variation of the magnetic properties with the resistance state, we explain the mechanism of resistive switching.

NiFe<sub>2</sub>O<sub>4</sub> thin films were prepared using a chemical solution deposition method. We synthesized the precursor solution using Ni(CH<sub>3</sub>COO)<sub>2</sub>·4H<sub>2</sub>O and Fe(NO<sub>3</sub>)<sub>3</sub>·9H<sub>2</sub>O as starting materials and 2-methoxyethanol and acetic acid as cosolvents. In brief, Ni(CH<sub>3</sub>COO)<sub>2</sub>·4H<sub>2</sub>O and Fe(NO<sub>3</sub>)<sub>3</sub>·9H<sub>2</sub>O at a Fe/Ni molar ratio of 2 were added to a 2:1 v/v mixture of 2-methoxyethanol and acetic acid to form the precursor solution (0.2 M). NiFe<sub>2</sub>O<sub>4</sub> thin films were prepared on Pt/Ti/SiO<sub>2</sub>/Si substrates by spin-coating the precursor solution at 3000 rpm for 30 s and baking at 300 °C for 5 min. The spin-coating was repeated eight times, and then the deposited films were annealed at 700 °C for 1 h in ambient air. The thickness of the obtained NiFe<sub>2</sub>O<sub>4</sub> thin films was ~350 nm. Structural characterizations (Figure S1 in the Supporting Information) by X-ray diffraction (XRD), scanning electron microscopy (SEM), and Raman spectroscopy indicated that the films had an inverse spinel nickel ferrite structure with a preferred (111)

Received: June 18, 2012

Published: August 29, 2012

orientation perpendicular to the surface of the substrate, and the films were smooth, crack-free, and uniform.

Initially, the as-prepared  $\text{NiFe}_2\text{O}_4$  thin films were always insulating with a high resistance. To investigate the resistive switching characteristics of Pt/ $\text{NiFe}_2\text{O}_4$ /Pt devices, an electroforming process, using a threshold current pulse of 10 mA, was performed to switch the device to the LRS. Figure 1a shows the

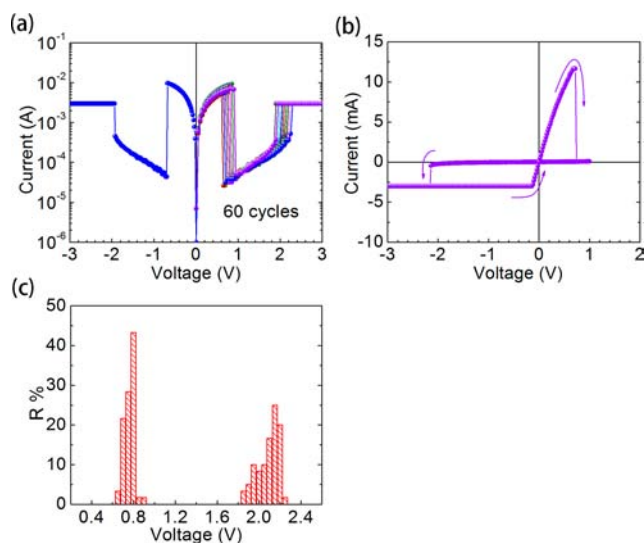


**Figure 1.** (a) Typical  $I$ – $V$  characteristics during repetitive switching cycles. (b) Typical  $I$ – $V$  characteristics under voltage sweeping (0 to 1 to  $-3$  to 0 V). (c) Distributions of the reset and set voltages for the Pt/ $\text{NiFe}_2\text{O}_4$ /Pt devices.

representative current–voltage ( $I$ – $V$ ) characteristics of the Pt/ $\text{NiFe}_2\text{O}_4$ /Pt devices during repetitive switching cycles. Unipolar resistive switching characteristics were clearly observed in both the forward- and backward-bias sweeping processes. Moreover, the right half of Figure 1a exhibits the reversible and reproducible resistive switching behavior, with high uniformity of the reset voltage ( $V_{\text{reset}}$ ), the set voltage ( $V_{\text{set}}$ ), low resistance, and high resistance during 60 successive cycles. When the forward voltage was increased to the critical voltage of 0.6–1.0 V, the current drastically decreased, indicating the switching of the Pt/ $\text{NiFe}_2\text{O}_4$ /Pt device from the LRS to the HRS. When the voltage was increased to a certain voltage in the range 1.8–2.2 V, soft breakdown occurred, and the device was switched from the HRS to the LRS. In addition, the resistive switching characteristics were also measured with reversal of the voltage polarity, as shown in Figure 1b. The switching from the LRS to the HRS occurred at positive bias and the switching from the HRS to the LRS at negative bias. The  $V_{\text{reset}}$ ,  $V_{\text{set}}$ , and resistance ratio values were similar to those in Figure 1a. Figure 1c shows the distributions of  $V_{\text{reset}}$  and  $V_{\text{set}}$  for resistive switching; the values were distributed in narrow ranges around  $0.8 \pm 0.2$  and  $2.0 \pm 0.2$  V, respectively. The results indicate that the switching parameters of the devices have excellent uniformity and a concentrated distribution of the operating voltages.

To address the reliability, the retention, endurance, and fatigue properties of the Pt/ $\text{NiFe}_2\text{O}_4$ /Pt devices were investigated. As shown in Figure 2a, the retention capabilities of the HRS and LRS were obtained under a readout voltage of 0.1 V every 10 s after the devices were switched to the HRS or LRS. The resistance values of both the HRS and LRS were stable without degradation over  $10^5$  s, indicating that the

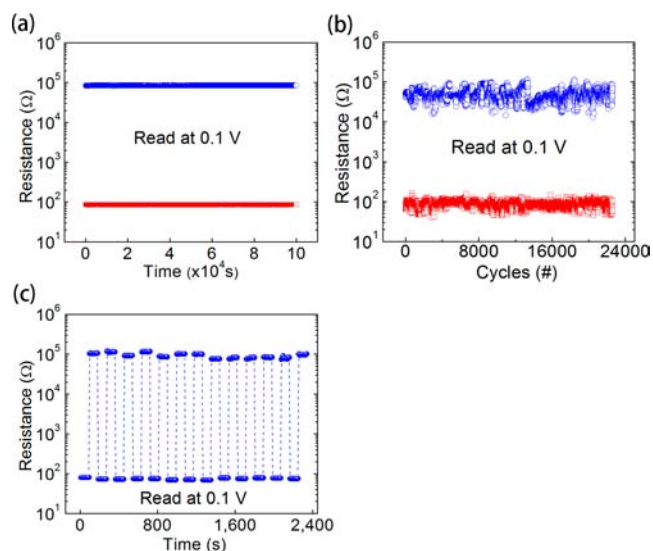


**Figure 2.** (a) Retention read at 0.1 V for the HRS (blue) and LRS (red), (b) switching cycles, and (c) fatigue characteristics of Pt/ $\text{NiFe}_2\text{O}_4$ /Pt devices.

devices are nonvolatile and can be read nondestructively. Figure 2b shows the resistive switching endurance of the Pt/ $\text{NiFe}_2\text{O}_4$ /Pt devices. Steady resistive switching characteristics over 22 500 cycles with small fluctuations in the HRS and LRS were observed. Figure 2c displays the fatigue characteristics of the Pt/ $\text{NiFe}_2\text{O}_4$ /Pt devices measured using a series of write/read/erase/read pulses with a readout voltage of 0.1 V, which also indicate that the two resistance states are stable.

To elucidate the conduction mechanism of resistive switching, the typical  $I$ – $V$  curves of the devices were plotted using a double-logarithmic scale, as in Figure 3a. The two straight lines are the fitting results. Evidently, the  $I$ – $V$  characteristic of the LRS showed a linear  $\log_{10}(I)$  versus  $\log_{10}(V)$  plot with a slope of  $\sim 1$ , indicating Ohmic behavior. However, the  $I$ – $V$  characteristic of the HRS was more complicated and could be

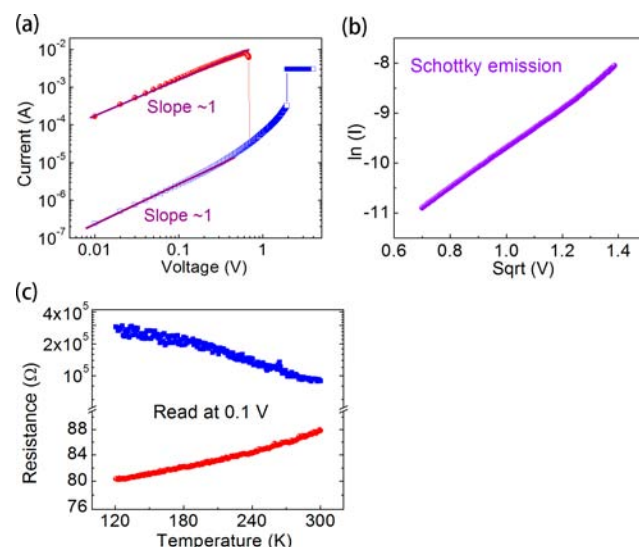


**Figure 3.** (a) Typical  $I$ – $V$  curves for resistive switching of the Pt/ $\text{NiFe}_2\text{O}_4$ /Pt devices plotted on a log–log scale. (b) Typical  $\ln(I)$  vs  $V^{1/2}$  plot for the higher-voltage region of the HRS. (c) Temperature dependence of the resistances of the HRS (blue) and LRS (red).

divided into two regions. In the lower-voltage range from 0 to 0.5 V, the  $I$ - $V$  characteristic showed a linear relation, corresponding to Ohmic behavior, whereas in the higher-voltage region of the HRS (0.5 V to  $V_{\text{set}}$ ), the  $I$ - $V$  curve showed a nonlinear relation, suggesting a different conducting mechanism. Further analysis indicated a linear relation between  $\ln(I)$  and  $V^{1/2}$ , as shown in Figure 3b, suggesting that Schottky emission is the dominant conduction mechanism in the higher-voltage region of the HRS.<sup>18–20</sup>

Figure 3c shows the temperature dependence of the LRS and HRS. The resistance of the HRS increased linearly with decreasing temperature, indicating insulating or semiconducting behavior in the HRS. In contrast, the resistance of the LRS increased with increasing temperature, indicating metallic conducting behavior. From a linear fit to the resistance of the LRS using the equation  $R(T) = R_0[1 + \alpha(T - T_0)]$ , the resistance temperature coefficient was determined to be  $\alpha = 5.6 \times 10^{-4} \text{ K}^{-1}$ . A similar resistance temperature coefficient was reported for InGaZnO resistive switching devices, and it was suggested that the conducting filaments were mainly composed of oxygen vacancies.<sup>21</sup>

Generally, a model involving formation and rupture of the conducting filaments can be used to explain the mechanism of unipolar resistive switching. According to this model, conducting filaments are formed by the electroforming process. The formation and rupture of the conducting filaments correspond to the set and reset processes, respectively, in the unipolar resistive switching. In the reset process, the conducting filaments rupture as a result of thermal and/or redox effects, and so on, whereas in the set process, the conducting filaments form again. Therefore, minimizing the random formation and rupture of the conducting filaments would improve the uniformity of the unipolar resistive switching. It has been reported that resistive switching devices with an active layer having enhanced crystallinity or highly preferred oriented growth show stable resistive switching parameters.<sup>22,23</sup> The enhanced crystallinity of the active layer can help stabilize the local domains for formation and rupture of the conducting filaments, resulting in the improved uniformity of resistive switching. While some defects such as oxygen vacancies tend to accumulate at the grain boundaries in highly oriented thin films after the electroforming process, the straight conducting filaments more easily form in films with a highly preferred orientation, which can minimize random connections and fracture during resistive switching.<sup>23</sup> In this study, the uniform resistive switching properties, including the stable operating voltages and small fluctuation in write/erase cycles, can also be ascribed to the strong crystallinity with preferentially (111)-oriented growth of the  $\text{NiFe}_2\text{O}_4$  thin films on Pt substrates. The conducting filaments mainly form at the grain boundaries along the preferential orientation direction.

Nickel ferrite,  $\text{NiFe}_2\text{O}_4$ , has the inverse spinel structure, with  $\text{Ni}^{2+}$  ions and half of the  $\text{Fe}^{3+}$  ions co-occupying octahedral sites (or B sites) and the other half of the  $\text{Fe}^{3+}$  ions occupying tetrahedral sites (or A sites). It has been reported that Fe–O bonds are stronger than Ni–O bonds<sup>24</sup> and that the formation energies of Fe vacancies are always larger than those of Ni vacancies, while oxygen vacancies have lower formation energies than Ni vacancies.<sup>24,25</sup> Therefore, oxygen vacancies form more easily than cationic vacancies do. Usually, few oxygen vacancies are formed during deposition under certain growth conditions.<sup>25</sup> Nevertheless, many more oxygen vacancies can be induced by electrical impulses during the

electroforming process. On the one hand, the oxygen vacancies may reduce some of the  $\text{Ni}^{2+}$  ions, leading to the formation of  $\text{Ni}^0$ ; on the other hand, it is also possible that the oxygen vacancies may reduce some of the  $\text{Fe}^{3+}$  ions to  $\text{Fe}^{2+}$  ions, changing the valence of some iron ions. Since half of the  $\text{Fe}^{3+}$  ions occupy A sites and the other half of the  $\text{Fe}^{3+}$  ions are in B sites in the  $\text{NiFe}_2\text{O}_4$  inverse spinel structure, we have to consider two cases: (i) the oxygen vacancies reduce  $\text{Fe}^{3+}$  ions in A sites to  $\text{Fe}^{2+}$  ions and (ii) the oxygen vacancies reduce  $\text{Fe}^{3+}$  ions in B sites to  $\text{Fe}^{2+}$  ions. In the former case, the total magnetic moment would be expected to increase. However, this would contradict the results of our magnetic measurements described in the following paragraph, so the reduction of  $\text{Fe}^{3+}$  ions in A sites can be ruled out. In the latter case, the total magnetic moment would be expected to decrease, in agreement with our magnetic measurements. In addition, there is the possibility of that some  $\text{Ni}^{2+}$  ions could migrate from B sites into A sites. However, if this were the case, the saturation magnetic moment would increase. This would also contradict our magnetic measurements. Thus, the case for migrating of  $\text{Ni}^{2+}$  ions from B sites into A sites can also be excluded. Therefore, the oxygen vacancies only reduce  $\text{Ni}^{2+}$  ions to  $\text{Ni}^0$  and  $\text{Fe}^{3+}$  ions to  $\text{Fe}^{2+}$  ions, both in B sites; that is, the oxygen vacancies change the valences of the cations in B sites.

To understand the role that oxygen vacancies and the reduction of cations play in the unipolar resistive switching mechanism, we investigated the magnetic properties of the fresh, LRS, and HRS samples. Figure 4a shows magnetic

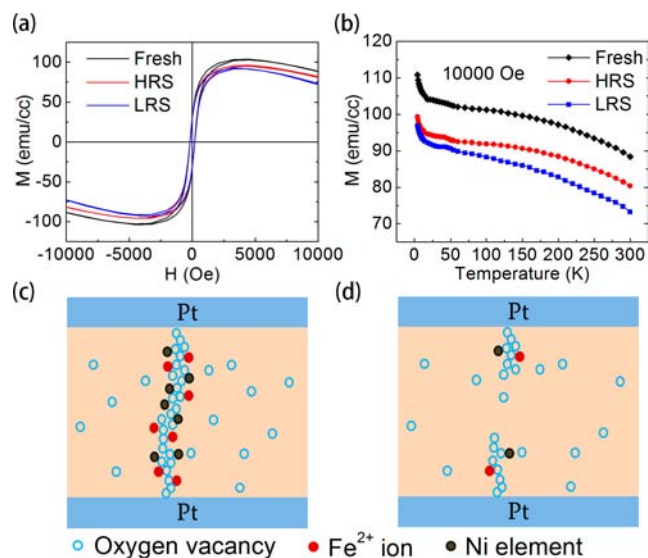


**Figure 4.** (a) Magnetic hysteresis loops at 300 K. (b) Temperature dependence of the magnetization of Pt/ $\text{NiFe}_2\text{O}_4$ /Pt devices with different resistance states. (c, d) Diagrams showing formation and rupture of conducting filaments in the LRS and HRS, respectively.

hysteresis loops for Pt/ $\text{NiFe}_2\text{O}_4$ /Pt devices in different resistance states at 300 K. The temperature dependence of the magnetization was also recorded at a magnetic field of 10 kOe, as shown in Figure 4b. All of the samples showed ferromagnetic behavior. The saturation magnetization ( $M_s$ ) of the fresh sample was greater than that of the HRS sample, and  $M_s$  of the HRS sample was greater than that of the LRS sample at 300 K. The variation of the magnetic properties of these samples with the resistance state may be attributed to the difference in the concentrations of oxygen vacancies and their

reduction effect in changing the valence of  $\text{Fe}^{3+}$  and  $\text{Ni}^{2+}$  ions.<sup>26,27</sup> Since the fresh sample contained a much smaller number of oxygen vacancies and/or reduced cations, its  $M_s$  should be larger than those of the HRS and LRS devices between 5 and 300 K, as indicated in Figure 4b. It should be noted that in Figure 4b, with decreasing temperature,  $M_s$  for the LRS sample gradually approached that of the HRS sample. It is known that in ferrite materials, oxygen vacancies lead to a substantial increase in the electrical conductivity,<sup>12,13</sup> similar to the case for our  $\text{NiFe}_2\text{O}_4$  thin films. The oxygen vacancies along with the reduction of cations give rise to excess electrons that get redistributed, and thus, the samples with oxygen vacancies exhibited increased conductivity and decreased  $M_s$ .<sup>12</sup> From Figure 4b, it can also be seen that  $M_s$  of the LRS sample gradually increased with decreasing temperature; correspondingly, in Figure 3c, the electrical resistance of the LRS sample slightly decreased (i.e., the conductivity increased) with decreasing temperature. Therefore, the approach of  $M_s$  for the LRS sample to that for the HRS sample at low temperature (several K) cannot be attributed to the effect of oxygen vacancies. Thus, the reduced cations might be responsible for increasing  $M_s$  of the LRS sample with decreasing temperature, causing its gradual approach to  $M_s$  for the HRS sample. Since both the HRS and fresh samples had few reduced cations, their magnetic properties exhibited almost the same trend.

In view of the observation that oxygen vacancies as well as reduction of cations could cause the decrease in magnetization and the increase in electrical conductivity in our thin films, combined with the results of the resistance–temperature measurements, it is rather reasonable to suggest that the conducting filaments in our thin films are composed of oxygen vacancies and reduced cations (or cations with changed valence). The filaments would rupture because of the annihilation of oxygen vacancies driven by the thermal effect and the changes in the valences of cations due to the redox effect in the reset process. Figure 4c,d describe the processes of formation and rupture, respectively, of the conducting filaments in our  $\text{NiFe}_2\text{O}_4$  thin films.

In conclusion, our Pt/ $\text{NiFe}_2\text{O}_4$ /Pt devices showed bistable unipolar resistive switching properties. The filament model can well explain the physical mechanism of resistive switching in terms of the thermal effect of oxygen vacancies and changes in the valences of cations due to the redox effect. Our results suggest that spinel ferrites can find opportunities in resistive random access memory applications.

## ■ ASSOCIATED CONTENT

### Ⓢ Supporting Information

XRD pattern, SEM images, Raman spectrum, and characterization methods. This material is available free of charge via the Internet at <http://pubs.acs.org>.

## ■ AUTHOR INFORMATION

### Corresponding Author

stsbdh@mail.sysu.edu.cn

### Notes

The authors declare no competing financial interest.

## ■ ACKNOWLEDGMENTS

The authors gratefully acknowledge financial support from the Natural Science Foundation of China (51172289), the Natural Science Fund of Guangdong Province, China

(10251027501000007), and the Specialized Research Fund for the Doctoral Program of Higher Education of China (20090171110007).

## ■ REFERENCES

- (1) Waser, R.; Dittmann, R.; Staikov, G.; Szot, K. *Adv. Mater.* **2009**, *21*, 2632.
- (2) Waser, R.; Aono, M. *Nat. Mater.* **2007**, *6*, 833.
- (3) Sawa, A. *Mater. Today* **2008**, *11*, 28.
- (4) Bao, D. H. *J. Ceram. Soc. Jpn.* **2009**, *117*, 929.
- (5) Chae, S. C.; Lee, J. S.; Kim, S.; Lee, S. B.; Chang, S. H.; Liu, C.; Kahng, B.; Shin, H.; Kim, D. W.; Jung, C. U.; Seo, S.; Lee, M. J.; Noh, T. W. *Adv. Mater.* **2008**, *20*, 1154.
- (6) Seo, S.; Lee, M. J.; Seo, D. H.; Jeoung, E. J.; Suh, D. S.; Joung, Y. S.; Yoo, I. K. *Appl. Phys. Lett.* **2004**, *85*, 5655.
- (7) Janousch, M.; Meijer, G. I.; Staub, U.; Delley, B.; Karg, S. F.; Andreasson, B. P. *Adv. Mater.* **2007**, *19*, 2232.
- (8) Chen, X. M.; Wu, G. H.; Bao, D. H. *Appl. Phys. Lett.* **2008**, *93*, No. 093501.
- (9) Sakamoto, T.; Sunamura, H.; Kawaura, H. *Appl. Phys. Lett.* **2003**, *82*, 3032.
- (10) He, C. L.; Zhuge, F.; Zhou, X. F.; Li, M.; Zhou, G. C.; Liu, Y. W.; Wang, J. Z.; Chen, B.; Su, W. J.; Liu, Z. P.; Wu, Y. H.; Cui, P.; Li, R. W. *Appl. Phys. Lett.* **2009**, *95*, No. 232101.
- (11) Lee, M. J.; Lee, C. B.; Lee, D.; Lee, S. R.; Chang, M.; Hur, J. H.; Kim, Y. B.; Kim, C. J.; Seo, D. H.; Chung, U. I.; Yoo, I. K.; Kim, K. *Nat. Mater.* **2011**, *10*, 625.
- (12) Anjum, S.; Jaffari, G. H.; Rumaiz, A. K.; Rafique, M. S.; Shah, S. I. *J. Phys. D: Appl. Phys.* **2010**, *43*, No. 265001.
- (13) Lüders, U.; Barthelemy, A.; Bibes, M.; Bouzehouane, K.; Fusil, S.; Jacquet, E.; Contour, J. P.; Bobo, J. F.; Fontcuberta, J.; Fert, A. *Adv. Mater.* **2006**, *18*, 1733.
- (14) Lüders, U.; Bibes, M.; Bobo, J. F.; Cantoni, M.; Bertacco, R.; Fontcuberta, J. *Phys. Rev. B* **2005**, *71*, No. 134419.
- (15) Lüders, U.; Herranz, G.; Bibes, M.; Bouzehouane, K.; Jacquet, E.; Contour, J.-P.; Fusil, S.; Bobo, J. F.; Fontcuberta, J.; Barthélémy, A.; Fert, A. *J. Appl. Phys.* **2006**, *99*, No. 08K301.
- (16) Chen, X. M.; Wu, G. H.; Jiang, P.; Liu, W. F.; Bao, D. H. *Appl. Phys. Lett.* **2009**, *94*, No. 033501.
- (17) Jin, C.; Jiang, E. Y.; Bai, H. L. *Appl. Surf. Sci.* **2011**, *257*, 8998.
- (18) Yan, Z. B.; Guo, Y. Y.; Zhang, G. Q.; Liu, J. M. *Adv. Mater.* **2011**, *23*, 1351.
- (19) Choi, B. J.; Jeong, D. S.; Kim, S. K.; Rohde, C.; Choi, S.; Oh, J. H.; Kim, H. J.; Hwang, C. S.; Szot, K.; Waser, R.; Reichenberg, B.; Tiedke, S. *J. Appl. Phys.* **2005**, *98*, No. 033715.
- (20) Szot, K.; Speier, W.; Carius, R.; Zastrow, U.; Beyer, W. *Phys. Rev. Lett.* **2002**, *88*, No. 075508.
- (21) Wang, Z. Q.; Xu, H. Y.; Li, X. H.; Zhang, X. T.; Liu, Y. X.; Liu, Y. C. *IEEE Electron Device Lett.* **2011**, *32*, 1442.
- (22) Kim, D. C.; Lee, M. J.; Ahn, S. E.; Seo, S.; Park, J. C.; Yoo, I. K. *Appl. Phys. Lett.* **2006**, *88*, No. 232106.
- (23) Liu, Z. J.; Chou, J. C.; Wei, S. Y.; Gan, J. Y.; Yew, T. R. *IEEE Electron Device Lett.* **2011**, *32*, 1728.
- (24) Perron, H.; Mellier, T.; Domain, C.; Roques, J.; Simoni, E.; Drot, R.; Catalette, H. *J. Phys.: Condens. Matter* **2007**, *19*, No. 346219.
- (25) Lee, H. D.; Kope, B. M.; Nishi, Y. *Phys. Rev. B* **2010**, *81*, No. 193202.
- (26) Son, J. Y.; Kim, C. H.; Cho, J. H.; Shin, Y. H.; Jang, H. M. *ACS Nano* **2010**, *4*, 3288.
- (27) Wu, S. X.; Li, X. Y.; Xing, X. J.; Hu, P.; Yu, Y. P.; Li, S. W. *Appl. Phys. Lett.* **2009**, *94*, No. 253504.